metals

Article

Effect of Substituting Hf for Zr on Fe-Co-M-Nb-B (M = Zr, Hf) Amorphous Alloys with High Saturation Magnetization

Hyunsol Son [1], Garam Yoo [1], Qoimatul Mustaghfiroh [2], Dong-Hyun Kim [2] and Haein Choi-Yim [1,*]

1 Department of Applied Physics, Sookmyung Women's University, Seoul 04310, Korea; 96gustof@sookmyung.ac.kr (H.S.); oenomel92@sookmyung.ac.kr (G.Y.)
2 Department of Physics, Chungbuk National University, Cheongju 28644, Korea; qoima@chungbuk.ac.kr (Q.M.); dhkim73@gmail.com (D.-H.K.)
* Correspondence: haein@sookmyung.ac.kr

Abstract: The soft magnetic amorphous ribbons of $(Fe_xCo_{1-x})_{85}M_9Nb_1B_5$ (M = Zr or Hf, x = 0.4, 0.5, 0.6, 0.7, 0.8, and 0.9) were investigated in this study. Replacing Zr by Hf turned out to increase saturation magnetization and, at the same time, reduce the coercivity, both of which serve together in enhancing the soft magnetic performance of the alloys. Moreover, the optimum ratio of Fe/Co was determined after the survey on different alloys with varying Fe/Co ratio resulting in the maximum saturation magnetization while keeping the coercivity low. After optimization, the highest saturation magnetization of 1.62 T was achieved with coercivity of 11 A/m. While substitution of Hf for Zr slightly reduced the crystallization onset temperature of the amorphous structure, the thermal stability of the soft magnetic amorphous alloys was not significantly affected by the Zr/Hf replacement.

Keywords: amorphous; soft magnetic properties; crystallization temperature; glass-forming ability

check for updates

Citation: Son, H.; Yoo, G.; Mustaghfiroh, Q.; Kim, D.-H.; Choi-Yim, H. Effect of Substituting Hf for Zr on Fe-Co-M-Nb-B (M = Zr, Hf) Amorphous Alloys with High Saturation Magnetization. *Metals* **2022**, *12*, 12. https://doi.org/10.3390/met12010012

Academic Editor: Imre Bakonyi

Received: 22 November 2021
Accepted: 19 December 2021
Published: 22 December 2021

Publisher's Note: MDPI stays neutral with regard to jurisdictional claims in published maps and institutional affiliations.

1. Introduction

There has been a significant interest in the various advantages of Fe-based amorphous alloys, such as good corrosion resistance, high fracture strength, and low material cost. Since the first Fe-based amorphous alloy of Fe-P-C was produced in 1967 [1], a variety of Fe-based amorphous alloys have been developed, such as Fe-Al-Ga-P-C-B [2], (Fe, Co, Ni)-P-B [3], (Fe, Co, Ni)-(Cr, Mo, W)-C [4], and (Fe, Co, Ni)-(Zr, Hf, Nb)-B [5,6]. Moreover, there are several studies for their commercial applications used in the electronics industry [7,8] to improve the soft magnetic properties, for example, high saturation magnetic flux density (B_s), low coercivity (H_c), and high permeability (μ_e) [9–13].

In particular, the Fe-rich Fe-Zr alloys attracted considerable attention in the past few years because of their spin-glass behavior [14,15]. However, Fe-Zr alloys in their binary composition with an amorphous structure are difficult to produce, which is a crucial requirement for soft magnetic performance [16,17]. It is well known that the small addition of B in Fe-Zr and Fe-Hf alloys improves their glass-forming ability (GFA). It has been reported that Fe-(Zr, Hf)-B alloys have a high Bs of 1.5 T and, at the same time, a wide compositional range for glass formation [5,16,17]. Furthermore, replacement of Zr by Hf decreased H_c in Fe-(Zr/Hf)-B alloys [18,19]. As another alloying element to increase the GFA of the Fe-based amorphous alloys, Nb plays important roles in amorphous alloys from different aspects: GFA, strength, and hardness [20]. Especially in the Fe-Zr-B system, small Nb addition enhanced the thermal stability while maintaining high B_s, low H_c, and high μ_e [21]. Moreover, appropriate substitution of Nb for Zr affected B_s, μ_e, and mean grain size [22,23]. As the last parameter to control the soft magnetic performance, Fe/Co ratio should be considered since it has been known that alloying Fe and Co together when producing Fe-Co-based amorphous metals resulted in improved saturation magnetization as well as higher GFA [8,24–26]. Indeed, by addition of B and Si [27] and B, Si, P, and C [28], Fe-Co-based amorphous alloys were recently reported to have outstanding saturation magnetization, 1.86 and 1.79 T, respectively. Combining the above-mentioned information reported so far, it is of high importance to survey the effect of Zr/Hf replacement and Fe/Co ratio in the same set of experimental schemes with an optimized composition of Nb, whose result is expected to suggest a new competitive soft magnetic alloy.

In this context, we report the effect of substitution of Hf for Zr with varying Fe/Co ratio in the $(Fe_xCo_{1-x})_{85}M_9Nb_1B_5$ (M = Zr or Hf, x = 0.4, 0.5, 0.6, 0.7, 0.8, and 0.9) alloys on magnetic and thermal properties.

2. Materials and Methods

Multi-component Fe-Co-based alloy ingots with nominal atomic percentage compositions of $(Fe_xCo_{1-x})_{85}M_9Nb_1B_5$ (M = Zr or Hf, x = 0.4, 0.5, 0.6, 0.7, 0.8, and 0.9) were prepared by using arc-melting under a Ti-gettered argon atmosphere with high purity metals of Fe (99.95%), Co (99.95%), B (99.5%), Si (99.999%), Nb (99.95%). Ingots were melted more than four times by flipping over the button-type ingot after every melting to maximize their compositional homogeneity. Ribbons with 2 mm width and 20 μm thickness were fabricated by using melt-spinning technique under an argon atmosphere with the rotational speed of a copper wheel of 56.3 m/s. The structure of the as-spun ribbons was analyzed by using X-ray diffraction (XRD, D8 Advance, Bruker, Billerica, MA, USA) with Cu-Kα radiation. The crystallization temperature (T_x) was measured by a differential scanning calorimeter (DSC, Labsys N-650, SCINCO, Seoul, Korea) under an argon atmosphere. Ribbons were heated from room temperature to 1100 K with a heating rate of 0.34 K/s. Magnetic properties such as B_s and H_c were measured by a vibrating sample magnetometer (VSM, EV9, MicroSense, Lowell, MA, USA) and a DC B-H loop tracer at room temperature (DC B-H loop tracer, MI-36, SENSORPIA Co., Ltd., Daejeon, Korea), respectively. B_s was measured by VSM under in-plane applied magnetic fields ranging from −800 to 800 kA/m. For VSM measurement, ribbons were cut in length of about 5 mm and 3 layers were used for a single measurement. H_c was measured by DC B-H loop tracer under maximum applied fields of 300 A/m. For B-H loop trancer, 5 layers of 100 mm long ribbons were used. Both VSM and DC B-H loop tracer can provide the information on the Hysteresis loop of materials under measurement. However, since H_c in soft magnetic amorphous materials is very small, H_c must be measured by a DC B-H loop tracer with a low field which has a better resolution. Magnetic domain observation was carried out by means of magneto-optical Kerr microscopy. Microscopic hysteresis loop, as well as corresponding magnetic domain patterns, are simultaneously investigated, where longitudinal magneto-optical Kerr effect is utilized to see the contrast [29].

3. Results and Discussion

Figure 1 shows XRD patterns of the $(Fe_xCo_{1-x})_{85}M_9Nb_1B_5$ (M = Zr or Hf, x = 0.4, 0.5, 0.6, 0.7, 0.8, and 0.9) melt-spun ribbons. For all specimens, typical pattern of amorphous structure characterized by a broad halo hump is observed. Although the lab-XRD is limited in detecting precipitation taking place in nanometer scale, XRD profiles of all samples suggest that those specimens prepared in this study are mostly composed of amorphous phase. A sharp peak with low intensity is observed for the case of $(Fe_xCo_{1-x})_{85}M_9Nb_1B_5$ (M = Hf, x = 0.9), however, based on its intensity compared to that of the amorphous hump, it appears that the fraction of the crystalline phase is not significant. Moreover, it could be noted that, for Figure 1b, where Hf was used, the broad hump became stronger as the Co concentration increased (as x decreased from 0.9 to 0.4). This observation suggests that higher fraction of Co compared to Fe in the case of Hf-added alloys could weaken GFA while mixing of Co and Fe in mutually comparable concentration leads to reasonable GFA of the alloys.

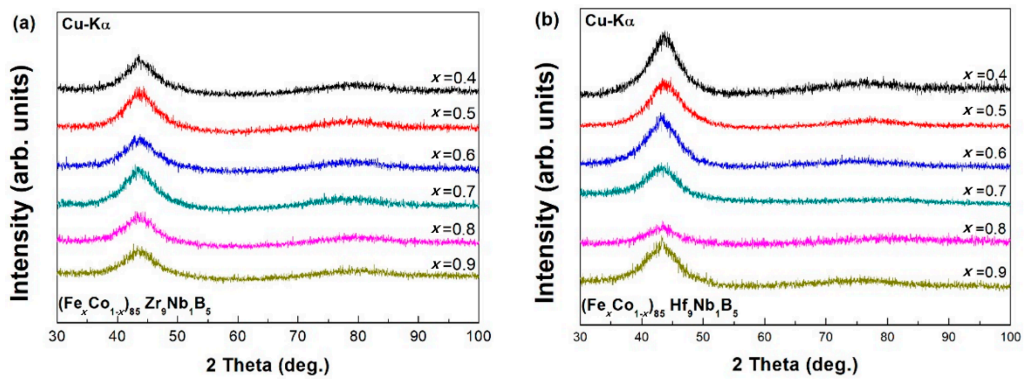

Figure 1. XRD patterns of the as-spun ribbons of (**a**) $(Fe_xCo_{1-x})_{85}Zr_9Nb_1B_5$ (alloys with Zr and x = 0.4, 0.5, 0.6, 0.7, 0.8, and 0.9) and (**b**) $(Fe_xCo_{1-x})_{85}Hf_9Nb_1B_5$ (alloys with Hf and x = 0.4, 0.5, 0.6, 0.7, 0.8, and 0.9).

Figure 2 shows the DSC thermograms of the $(Fe_xCo_{1-x})_{85}M_9Nb_1B_5$ (M = Zr or Hf, x = 0.4, 0.5, 0.6, 0.7, 0.8, and 0.9) melt-spun ribbons, and the crystallization onset temperatures (T_x) of the alloys were marked by arrows. With increasing Fe content, T_x of the $(Fe_xCo_{1-x})_{85}Zr_9Nb_1B_5$ (alloys with Zr and x = 0.4, 0.5, 0.6, 0.7, 0.8, and 0.9) and $(Fe_xCo_{1-x})_{85}Hf_9Nb_1B_5$ (alloys with Hf and x = 0.4, 0.5, 0.6, 0.7, 0.8, and 0.9) as-spun ribbons was also increasing from 819 to 858 K and from 808 to 849 K, respectively. These values of the T_x for all alloys are shown in Table 1. For a given ratio of Fe/Co, T_x of the alloy with Zr is higher than that of the Hf case, which suggests the enhanced thermal stability induced by Zr substitution for Hf.

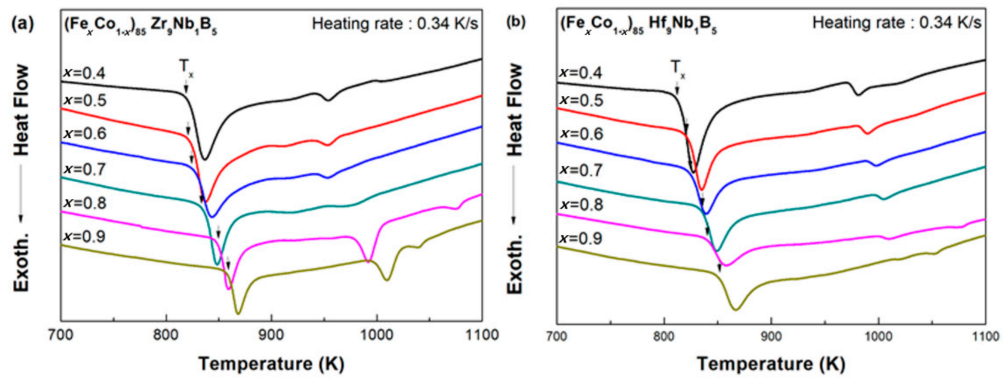

Figure 2. DSC curves of the as-spun ribbons of (**a**) $(Fe_xCo_{1-x})_{85}Zr_9Nb_1B_5$ (alloys with Zr and x = 0.4, 0.5, 0.6, 0.7, 0.8, and 0.9) and (**b**) $(Fe_xCo_{1-x})_{85}Hf_9Nb_1B_5$ (alloys with Hf and x = 0.4, 0.5, 0.6, 0.7, 0.8, and 0.9).

The magnetic properties were analyzed by measuring hysteresis loops. Hysteresis loops (B-H curves) of the $(Fe_xCo_{1-x})_{85}M_9Nb_1B_5$ (M = Zr or Hf, x = 0.4, 0.5, 0.6, 0.7, 0.8, and 0.9) melt-spun ribbons were obtained by using VSM as shown in Figure 3. VSM measured the B_s values, and the H_c values were measured by DC B-H loop tracer. All of the hysteresis loops are shown as typical B-H loops of soft magnetic amorphous materials.

All of the B_s and H_c values are summarized in Table 1. The B_s and H_c of the Metglas 2605 CO, a common amorphous material, are 1.2 T and 80 A/m, respectively. Moreover, for 30KCP ($Fe_{57}Co_{26}Cr_3B_{14}C_{0.2}$ metallic glass), it has been reported that B_s is 1.3 T, and H_c is 80 A/m [30]. Compared to these values, the Fe-Co-(Zr/Hf)-Nb-B alloys used in this study turned out to have better soft magnetic properties.

Table 1. Thermal and magnetic properties of $(Fe_xCo_{1-x})_{85}M_9Nb_1B_5$ (M = Zr or Hf, x = 0.4, 0.5, 0.6, 0.7, 0.8, and 0.9) as-spun ribbons.

Alloys						Thermal Properties	Magnetic Properties	
Fe/Co Ratio	Alloy Composition					T_x (K)	H_c (A/m)	B_s (T)
4:6	Fe_{34}	Co_{51}	Zr_9	Nb_1	B_5	819	24	1.22
5:5	$Fe_{47.5}$	$Co_{47.5}$	Zr_9	Nb_1	B_5	822	22	1.33
6:4	Fe_{51}	Co_{34}	Zr_9	Nb_1	B_5	827	21	1.52
7:3	$Fe_{59.5}$	$Co_{25.5}$	Zr_9	Nb_1	B_5	837	18	1.48
8:2	Fe_{68}	Co_{17}	Zr_9	Nb_1	B_5	850	15	1.38
9:1	$Fe_{76.5}$	$Co_{8.5}$	Zr_9	Nb_1	B_5	858	12	1.19
4:6	Fe_{34}	Co_{51}	Hf_9	Nb_1	B_5	808	23	1.43
5:5	$Fe_{47.5}$	$Co_{47.5}$	Hf_9	Nb_1	B_5	817	20	1.62
6:4	Fe_{51}	Co_{34}	Hf_9	Nb_1	B_5	823	19	1.54
7:3	$Fe_{59.5}$	$Co_{25.5}$	Hf_9	Nb_1	B_5	832	17	1.40
8:2	Fe_{68}	Co_{17}	Hf_9	Nb_1	B_5	839	14	1.18
9:1	$Fe_{76.5}$	$Co_{8.5}$	Hf_9	Nb_1	B_5	849	11	0.93

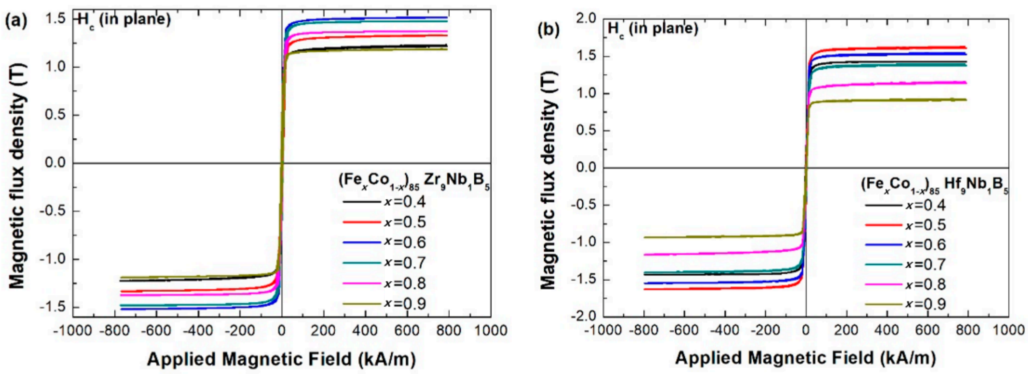

Figure 3. Hysteresis loops of the as-spun ribbons measured by VSM of (**a**) $(Fe_xCo_{1-x})_{85}Zr_9Nb_1B_5$ (alloys with Zr and x = 0.4, 0.5, 0.6, 0.7, 0.8, and 0.9) and (**b**) $(Fe_xCo_{1-x})_{85}Hf_9Nb_1B_5$ (alloys with Hf and x = 0.4, 0.5, 0.6, 0.7, 0.8, and 0.9).

Figure 4 shows variation of the B_s and H_c of $(Fe_xCo_{1-x})_{85}M_9Nb_1B_5$ (M = Zr or Hf, x = 0.4, 0.5, 0.6, 0.7, 0.8, and 0.9) as-spun ribbons. B_s of Fe-Co-Hf-Nb-B as-spun ribbons has a wider variation than that of Fe-Co-Zr-Nb-B, as shown in Figure 4a. The highest value of B_s was 1.62 T with $Fe_{47.5}Co_{47.5}Hf_9Nb_1B_5$ (M = Hf and x = 0.5) amorphous ribbon, and the lowest was 0.93 T of $Fe_{76.5}Co_{8.5}Hf_9Nb_1B_5$ (M = Hf and x = 0.9). Moreover, from Figure 4a, we can determine the optimum ratio of each alloy system. The optimum Fe/Co ratios are 5/5 and 6/4 for Hf- and Zr-added alloys, respectively. The observed behavior also agrees with the previous report on Fe-Co-based alloys claiming the improvement in B_s by mixing Fe and Co rather than having Fe-only or Co-only alloys [6].

For the variation of H_c shown in Figure 4b, monotonous decrease in H_c for both groups of alloys was observed with increases in Fe/Co ratio: from 24 to 12 A/m and from 23 to 11 A/m for Zr- and Hf-added alloys, respectively. In all of the compositions, the Fe-Co-Hf-Nb-B alloys have lower H_c than the alloys with Zr for every given ratio of Fe/Co. This could be attributed to the difference in amorphous structure: as shown in Figure 1b, Hf-added alloys could have lower crystallinity (evidenced by slight crystallinity shown for the case of x = 0.9) which was also discussed in the context of 'quenched-in-disorder' [31,32]. Therefore, it is evident that the substitution of Hf for Zr induces lower H_c values.

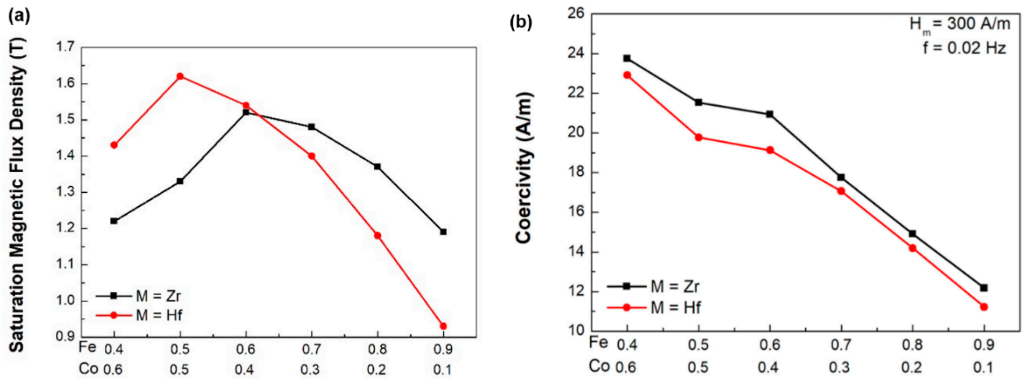

Figure 4. (**a**) Variation of the saturation magnetization (B_s) and (**b**) coercivity (H_c) of the as-spun ribbons of $(Fe_xCo_{1-x})_{85}M_9Nb_1B_5$ (M = Zr or Hf, x = 0.4, 0.5, 0.6, 0.7, 0.8, and 0.9).

We have carried out direct observation of magnetic domain patterns with Fe/Co ratio variation, as shown in Figure 5, where domain patterns and corresponding microscopic hysteresis loops for the cases of x = 0.5 and 0.9 for $(Fe_xCo_{1-x})_{85}Hf_9Nb_1B_5$ alloys are illustrated. In case of x = 0.9 (Figure 5a), the domain pattern is significantly simpler compared to the case of x = 0.5 (Figure 5b) with a configuration of 180° domain wall. The microscopic hysteresis loop corresponding to the observed area when x = 0.9 shows a stepwise behavior both in increasing and decreasing branches. The observed patterns are consistent with the structural properties in Figure 1b, where a relatively narrow XRD peak in case of x = 0.9 probably promotes a simpler domain pattern. On the other hand, the domain pattern becomes more complex in case of x = 0.5 as seen in Figure 5b. The corresponding microscopic hysteresis does not exhibit a stepwise jump behavior but shows a gradual change with dispersion around the coercivity. It should be also mentioned that the rather complex domain patterns are matching with the saturation magnetization results in Figure 4a, where the highest saturation magnetization might lead to the highest magnetostatic energy, generally resulting in more complex domain patterns.

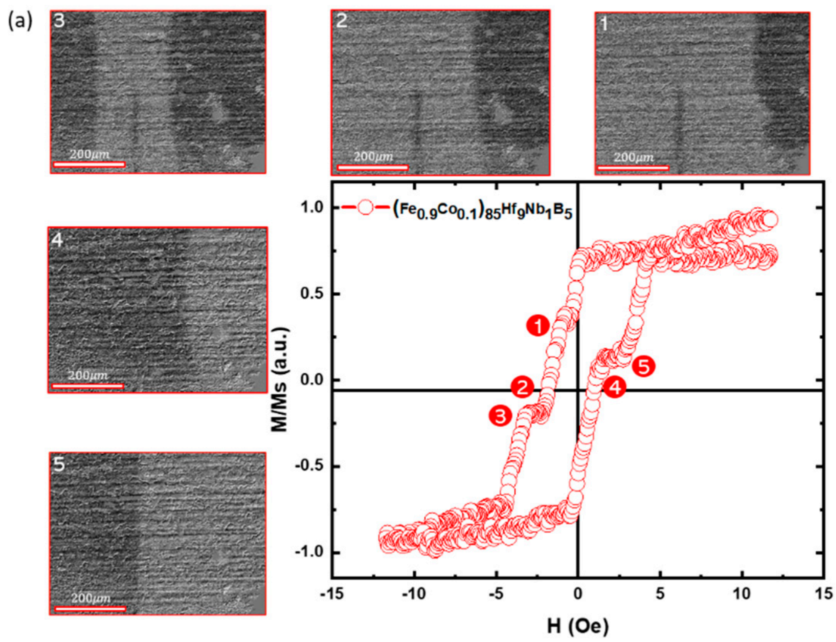

Figure 5. *Cont.*

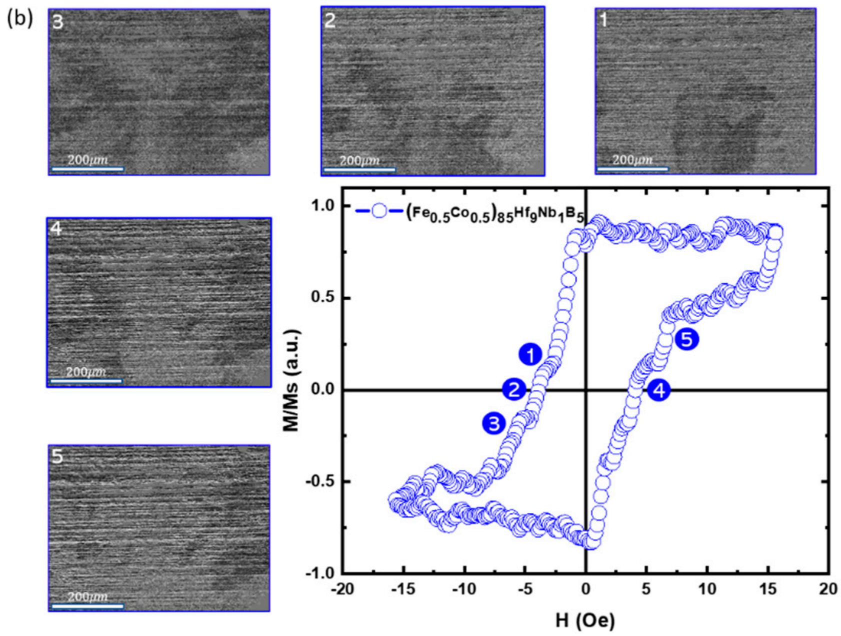

Figure 5. Magnetic domain observation result and corresponding microscopic hysteresis loops for $(Fe_xCo_{1-x})_{85}Hf_9Nb_1B_5$ alloys with (**a**) x = 0.9 and (**b**) 0.5.

This study discussed the effect of substitution of Zr for Hf by varying the ratio of Fe/Co on thermal and magnetic properties. T_x decreases when Zr is replaced by Hf, whereas the magnetic properties of B_s and H_c improve. B_s has a wider range of variation in the Fe-Co-Hf-Nb-B alloys compared to the Fe-Co-Zr-Nb-B alloys, so the highest and the lowest values are found in the Fe-Co-Hf-Nb-B alloys. Especially, it should be noted that the highest value of B_s obtained in this study is 1.62 T, which is a significantly competitive value in soft magnetic amorphous materials. Moreover, all of the H_c values of the Fe-Co-Hf-Nb-B alloys are lower than those of the Fe-Co-Zr-Nb-B alloys for all the given ratio of Fe/Co, suggesting another positive effect of the Hf substitution.

4. Conclusions

In this study, we observed the effect of substituting Hf for Zr with the Fe/Co ratio variation in the Fe-Co-(Zr/Hf)-Nb-B alloys on saturation magnetization (B_s), coercivity (H_c), and crystallization temperature (T_x). Magnetic and thermal properties of the Fe-Co-(Zr/Hf)-Nb-B alloys were measured by VSM, DC B-H loop tracer, and DSC. The results of this study can be summarized as follows:

(a) The effects of substituting Hf for Zr on T_x, B_s, and H_c values are noted as follows. The T_x decreased for every given Fe/Co ratio by incorporating Hf. The variation of B_s is increased by the incorporation of Hf so that both the highest and the lowest B_s values are observed in the Fe-Co-Hf-Nb-B alloys. Particularly, the highest B_s is 1.62 T in $Fe_{47.5}Co_{47.5}Hf_9Nb_1B_5$ (M = Hf and x = 0.5) amorphous ribbon. Moreover, the H_c decreases by substituting Hf for Zr for every given Fe/Co ratio. The lowest H_c value is 11 A/m in $Fe_{76.5}Co_{8.5}Hf_9Nb_1B_5$ (M = Hf and x = 0.9) melt-spun ribbon. Therefore, the soft magnetic properties, both B_s and H_c, are enhanced by substituting Hf for Zr.

(b) The effects of varying the Fe/Co ratio from 4/6 to 9/1 on thermal and magnetic properties are noted as follows. The T_x increases gradually from 819 to 858 K and from 808 to 849 K in the Zr- and Hf-added alloys, respectively, with the increase in the ratio of Fe/Co from 4/6 to 9/1, suggesting that the Fe/Co ratio affects the thermal stability of the alloys. The optimum Fe/Co ratios for maximizing B_s are 6/4 for the Fe-Co-Zr-Nb-B alloys and 5/5 for the Fe-Co-Hf-Nb-B alloys. The H_c decreases continuously from 24 to 12 A/m for the Fe-Co-Zr-Nb-B alloys and 23 to 11 A/m for the Fe-Co-Hf-Nb-B alloys with the variation of Fe/Co ratio from 4/6 to 9/1. As a result, it can be concluded that the values of T_x and H_c depend on Fe/Co ratio, and the optimum mixing ratio of Fe/Co achieves the maximum saturation magnetization (B_s).

In conclusion, the $(Fe_xCo_{1-x})_{85}M_9Nb_1B_5$ (M = Zr or Hf, x = 0.4, 0.5, 0.6, 0.7, 0.8, and 0.9) alloys studied in this report have excellent soft magnetic properties and high thermal stability, which suggests that they can be used in various commercial applications.

Author Contributions: Conceptualization, H.C.-Y.; methodology, G.Y., H.S. and Q.M.; validation, H.S.; formal analysis, G.Y., H.S. and D.-H.K.; investigation, G.Y., H.S. and Q.M.; resources, G.Y.; data curation, H.S. and G.Y.; writing—original draft preparation, G.Y. and H.S.; writing—review and editing, H.S.; visualization, H.S.; supervision, H.C.-Y.; project administration, H.C.-Y.; funding acquisition, H.C.-Y. All authors have read and agreed to the published version of the manuscript.

Funding: This work was supported by the Technology Innovation Program (Material Parts Technology Development-Material Parts Package-Type Technology Development Project) (20011368, Development of Thin Film Technology on Soft Magnetic Steel Sheet and Application Technology on Hybrid Permanent Magnet for High Performance Traction Motor) funded By the Ministry of Trade, Industry & Energy (MOTIE, Korea).

Data Availability Statement: No new data were created or analyzed in this study. Data sharing is not applicable to this article.

Conflicts of Interest: The authors declare no conflict of interest.

References

1. Duwez, P.; Lin, S.C.H. Amorphous ferromagnetic phase in iron-carbon-phosphorus alloys. *J. Appl. Phys.* **1967**, *38*, 4096–4097. [CrossRef]
2. Mizushima, T.; Makino, A.; Inoue, A. Structure and magnetic properties of Fe-based glassy alloys. *Mater. Sci. Eng. A* **1997**, *226*, 721–725. [CrossRef]
3. Hasegawa, R. Spin-fluctuation resistivity in alloys. *Phys. Lett. A* **1972**, *38*, 5–7. [CrossRef]
4. Masumoto, T.; Waseda, Y.; Kimura, H.; Inoue, A. Structural stability of amorphous metals. *Sci. Rep. Res. Inst. Tohoku Univ. Ser. A Phys. Chem. Metall.* **1976**, *26*, 96. [CrossRef]
5. Inoue, A.; Kobayashi, K.; Nose, M.; Masumoto, T. Mechanical properties of (Fe, Co, Ni)-MB (M = Ti, Zr, Hf, V, Nb, Ta and Mo) amorphous alloys with low boron concentration. *J. Phys. Colloq.* **1980**, *41*, C8-831–C8-834. [CrossRef]
6. Han, B.; Kim, Y.K.; Choi-Yim, H. Effect of compositional variation on the soft magnetic properties of $Fe_{(87-x-y)}Co_xTi_7Zr_6B_y$ amorphous ribbons. *Curr. Appl. Phys.* **2014**, *14*, 685–687. [CrossRef]
7. Inoue, A.; Wang, X.M.; Zhang, W. Developments and Applications of Bulk Metallic Glasses. *Rev. Adv. Mater. Sci.* **2008**, *18*, 1–9.
8. Chang, H.W.; Huang, Y.C.; Chang, C.W.; Hsieh, C.C.; Chang, W.C. Soft magnetic properties and glass formability of Y–Fe–B–M bulk metals (M = Al, Hf, Nb, Ta, and Ti). *J. Alloys Compd.* **2009**, *472*, 166–170. [CrossRef]
9. Inoue, A.; Shen, B.L.; Chang, C.T. Super-high strength of over 4000 MPa for Fe-based bulk glassy alloys in $[(Fe_{1-x}Co_x)_{0.75}B_{0.2}Si_{0.05}]_{96}Nb_4$ system. *Acta Mater.* **2004**, *52*, 4093–4099. [CrossRef]
10. Shen, B.; Inoue, A.; Chang, C. Superhigh strength and good soft-magnetic properties of (Fe, Co)–B–Si–Nb bulk glassy alloys with high glass-forming ability. *Appl. Phys. Lett.* **2004**, *85*, 4911–4913. [CrossRef]
11. Shen, B.; Chang, C.; Kubota, T.; Inoue, A. Superhigh strength and excellent soft-magnetic properties of $[(Co_{1-x}Fe_x)_{0.75}B_{0.2}Si_{0.05}]_{96}Nb_4$ bulk glassy alloys. *J. Appl. Phys.* **2006**, *100*, 013515. [CrossRef]
12. Matsubara, E.; Tamura, T.; Waseda, Y.; Inoue, A.; Zhang, T.; Masumoto, T. Structural study of $Zr_{60}Al_{15}Ni_{25}$ amorphous alloys with a wide supercooled liquid region by the anomalous X-ray scattering (AXS) method. *Mater. Trans. JIM* **1992**, *33*, 873–878. [CrossRef]
13. Inoue, A.; Takeuchi, A.; Zhang, T.; Murakami, A.; Makino, A. Soft magnetic properties of bulk Fe-based amorphous alloys prepared by copper mold casting. *IEEE Trans. Magn.* **1996**, *32*, 4866–4871. [CrossRef]
14. Hiroyoshi, H.; Fukamichi, K. Ferromagnetic-spin glass transition in Fe-Zr amorphous alloy system. *J. Appl. Phys.* **1982**, *53*, 2226–2228. [CrossRef]
15. Ennas, G.; Magini, M.; Padella, F.; Susini, P.; Boffitto, G.; Licheri, G. Preparation of amorphous Fe-Zr alloys by mechanical alloying and melt spinning methods. *J. Mater. Sci.* **1989**, *24*, 3053–3058. [CrossRef]
16. Ohnuma, S.; Masateru, N.; Kiwamu, S. Magnetic properties of amorphous Fe-Zr-B alloys. *Sci. Rep. Res. Inst. Tohoku Univ. Ser. A Phys. Chem. Metall.* **1980**, *29*, 254–264.
17. Masumoto, T.; Ohnuma, S.; Shirakawa, K.; Nose, M.; Kobayashi, K. Magnetic properties of metal-metal amorphous alloys. *J. Phys. Colloq.* **1980**, *41*, C8-686–C8-689. [CrossRef]
18. Suzuki, K.; Makino, A.; Inoue, A.; Masumoto, T. Soft magnetic properties of nanocrystalline bcc Fe-Zr-B and Fe-M-B-Cu (M = transition metal) alloys with high saturation magnetization. *J. Appl. Phys.* **1991**, *70*, 6232–6237. [CrossRef]

19. Makino, A.; Suzuki, K.; Inoue, A.; Hirotsu, Y.; Masumoto, T. Magnetic properties and microstructure of nanocrystalline bcc Fe-MB (M = Zr, Hf, Nb) alloys. *J. Magn. Magn. Mater.* **1994**, *133*, 329–333. [CrossRef]
20. Ma, L.; Wang, L.; Zhang, T.; Inoue, A. Effect of Nb addition on glass-forming ability, strength, and hardness of Fe–B–Zr amorphous alloys. *Mater. Res. Bull.* **1999**, *34*, 915–920. [CrossRef]
21. Inoue, A.; Shen, B. New Fe-based bulk glassy alloys with high saturated magnetic flux density of 1.4–1.5 T. *Mater. Sci. Eng. A* **2004**, *375*, 302–306. [CrossRef]
22. Makino, A.; Bitoh, T.; Kojima, A.; Inoue, A.; Masumoto, T. Magnetic properties of zero-magnetostrictive nanocrystalline Fe–Zr–Nb–B soft magnetic alloys with high magnetic induction. *J. Magn. Magn. Mater.* **2000**, *215*, 288–292. [CrossRef]
23. Makino, A.; Hatanai, T.; Naitoh, Y.; Bitoh, T.; Inoue, A.; Masumoto, T. Applications of nanocrystalline soft magnetic Fe-MB (M= Zr, Nb) alloys "NANOPERM (R)". *IEEE Trans. Magn.* **1997**, *33*, 3793–3798. [CrossRef]
24. Inoue, A. Stabilization of metallic supercooled liquid and bulk amorphous alloys. *Acta Mater.* **2000**, *48*, 279–306. [CrossRef]
25. Itoi, T.; Inoue, A. Thermal stability and soft magnetic properties of Co–Fe–M–B (M = Nb, Zr) amorphous alloys with large supercooled liquid region. *Mater. Trans. JIM* **2000**, *41*, 1256–1262. [CrossRef]
26. Wang, J.; Wang, Z.; Jia, Y.Y.; Shi, R.M.; Wen, Z.P. High temperature soft magnetic properties of $(Fe_xCo_{1-x})_{73.5}Cu_1Mo_3Si_{13.5}B_9$ (x = 0.5, 1) alloys. *J. Magn. Magn. Mater.* **2013**, *328*, 62–65. [CrossRef]
27. Wang, F.; Inoue, A.; Han, Y.; Kong, F.L.; Zhu, S.L.; Shalaan, E.; Al-Marzouki, F.; Obaid, A. Excellent soft magnetic Fe-Co-B-based amorphous alloys with extremely high saturation magnetization above 1.85 T and low coercivity below 3 A/m. *J. Alloys Compd.* **2017**, *711*, 132–142. [CrossRef]
28. Shi, Z.; Li, R.; Zhang, T. Tunable magnetic properties and heat-treatable bending ductility of Fe-Co-BPC amorphous alloys with a high saturated magnetization up to 1.79 T. *J. Alloys Compd.* **2019**, *778*, 302–308. [CrossRef]
29. Kim, D.H.; Choe, S.B.; Shin, S.C. Direct observation of Barkhausen avalanche in Co thin films. *Phys. Rev. Lett.* **2003**, *90*, 087203. [CrossRef] [PubMed]
30. Mamaev, G.; Bolotin, I.; Ctcherbakov, A.; Mamaev, S.; Poutchkov, S.; Tenyakov, I. Technology for production of amorphous alloys large scale cores. In Proceedings of the 1997 Particle Accelerator Conference (Cat. No. 97CH36167), Vancouver, BC, Canada, 16 May 1997; pp. 1313–1315.
31. Horvat, J.; Babi, E.; Marohni, Ž.; Liebermann, H.H. Domain wall stabilization in Co74Fe6B20 amorphous alloys. *Philos. Mag. B* **1991**, *63*, 1235–1245. [CrossRef]
32. Horvat, J.; Babić, E. The variation of the domain wall pinning strength with the depth within the $Co_{74}Fe_6B_{20}$ amorphous alloy. *J. Magn. Magn. Mater.* **1991**, *96*, L13–L16. [CrossRef]